

AlCoCrFeNiTi and its equal-molar five-component alloys in a metal mixological enthalpy-entropy plane

Authors:

Swe-Kai Chen¹
Po-Han Lee²
Chuan-Hsiang Lin¹

Affiliations:

1. Center for Nanotechnology, Materials Science, and Microsystems, National Tsing Hua University, Hsinchu 30013, Taiwan
2. Affiliated Senior High School of National Taiwan Normal University, Taipei 10658, Taiwan

E-mails:

skchen@mx.nthu.edu.tw
phlee@hs.ntnu.edu.tw
mstedodo@hotmail.com

Abstract

High-entropy alloys (HEAs) study has become a mature and profound field in the alloy world. We review the high-entropy alloys of equal-molar AlCoCrFeNiTi and its six five-component alloys such as equal-molar AlCoCrFeNi (Ti-free) etc. by considering every possible combination of elements. Whether a phase is a solid solution or an intermetallic compound is examined by a mixing entropy-enthalpy plane that is referred to as a MEE plane. The phases existences in the HEAs are verified by experiments and the four core effects are also checked. According to experiments in the residual resistivity ratio of some HEAs that approaches unity in a wide range of temperatures, the fifth effect that the unit cell of an HEA pseudo-unitary lattice possesses a 'saturation density of point defects' is added to the four core effects of HEAs.

1. Introduction

Undoubtedly, the invention of multi-principal-component or high-entropy alloys (MCAs or HEAs) is a milestone in the historical development of alloys since they provide large degrees of freedom in alloy designs and applications.¹⁻⁴ HEAs are defined as alloys containing at least five major elements, each of which has a concentration range between 5 and 35 at.%, and with high mixing entropy in their liquid state or high-temperature solid solution state. The many promising properties of HEA have been reported, such as outstanding wear resistance,⁵ high hardness,⁶⁻¹⁰ excellent high-temperature strength,^{11,12} good thermal stability,¹³ corrosion resistance,^{14,15} formation of nanostructures,^{16,17} high yield and fracture strengths,¹⁸ low-temperature fracture resistance,¹⁹ and special near-zero thermal coefficient of electrical resistivity.²⁰ They provide great potentiality in materials selection and applications.³

1.1. Review on AlCoCoCrFeNi+Ti HEA system

There are four phases for $\text{Al}_x\text{CoCrFeNi}$ alloys in $x = 0 - 1.8$.²¹ Even in $\text{Al}_{0.5}\text{CoCrCuFeNiTi}_x$ ($x = 0 - 2$) only a few phases exist.²² There is a superior room-temperature compression effect in $\text{AlCoCrFeNiTi}_{1.5}$.⁷ $\text{Al}_{0.5}\text{Co}_x\text{CrFeNiTi}$ show a microstructural change from two BCCs to a mix of BCC and FCC, and there is a slight

inferiority in compressive strength as x rises.²³ A phase transition from face-centered cubic (FCC) of $\text{CrFeCoNiAl}_{0.5}\text{Cu}_{0.5}$ alloy to body-centered cubic (BCC) of $\text{CrFeCoNiAl}_{0.75}\text{Cu}_{0.25}$ is ascribed to lattice distortion.²⁴

$\text{Al}_x\text{CoCrFeNiTi}$ show good ambient mechanical properties, the optimum compressive strength and elastic modulus appear at $x = 1$.²⁵ The high-entropy strategy may be applied to a wide range of complex materials²⁶. Mechanically alloyed and sintered AlCoCrFeNiTi has a crystal size of 40 nm and shows hardness of HV 432.¹⁷ CoCrFeNiTi_x give HV from 135 to 515; the higher the x , the higher the HV.²⁷ The dendrite in as-cast $\text{Al}_{0.5}\text{CoCrNiTi}_{0.5}$ is made of a duplex FCC-BCC, the highest HV is 743.²⁸ Even CrCoNi is able to illustrate the exceptional damage-tolerance at cryogenic temperatures.²⁹ $\text{Co}_{1.5}\text{CrFeNi}_{1.5}\text{Ti}$ and $\text{Al}_{0.2}\text{Co}_{1.5}\text{CrFeNi}_{1.5}\text{Ti}$ show excellent anti-oxidation and resistance to thermal softening for the outstanding wear resistance.⁵ Ti in $\text{Al}_{0.3}\text{CoCrFeNiTi}_{0.1}$ exhibits an apparent age hardening at 700 °C.³⁰ The hardness of $\text{Al}_{0.5}\text{CoCrFeNi}$ increases after aging.³¹ Single crystal $\text{Al}_{0.3}\text{CoCrFeNi}$ illustrates superior tensile elongation.^{32,33}

1.2. The core effects of HEAs

The outstanding properties of high-entropy alloys are directly related to the core effects. They result from the

fundamentals of HEAs. Under the assumption of a reversible condition of $\Delta H = T\Delta S$ (i.e., $\Delta G = 0$) for any reaction and from the fact that small $|\Delta H|$ usually implies high solubility of alloying elements, one can plot a ΔH - $T\Delta S$ plane to elucidate the extension of ΔH for high solubility under the effect of $T\Delta S$.³⁴ The extension in solubility of alloy components is an effect of high entropy on alloys. Obviously, the most effective ways for achieving high entropy conditions are both activating temperatures to a reasonably high temperature and adding multiple elements in an alloy. The first condition occurs in the melting process of forming alloys; the second condition of multiprincipal elements defines HEAs. The extension in component solubility enables HEAs to form a single, simple unitary lattice (UL) like that happens in elements. UL is the characteristic lattice for any high-entropy alloy (HEA), giving the high lattice distortion effect, the slow diffusion effect,³⁵ and the cocktail effect,¹ as well as a high dense point-defect in a single UL. The high lattice distortion effect originates from the wide range of atomic sizes in a UL. The diffusion of component atoms as that of a whole of a UL gives the slow diffusion effect. Thus, UL is the DNA of HEAs; as a result, they show the cocktail effect. From the experimental results of the residual resistivity ratio that approaches unity for most HEAs results in UL possessing a high density of point defects in itself.²⁰ There are various counterpart

effects and applications for HEAs as to the corresponding ones in conventional alloys.

1.3. Entropy-enthalpy plane

Enthalpy is by no means the only decisive factor for alloy forming; entropy is yet another important factor due to the existence of multi-principal-component. Viewing their 'equal' effect on alloys, it is necessary to consider both of them in researching properties of HEAs.³⁶ The changed phase in the process of HEA is able to reflect some of the characteristics of thermodynamics,^{37,38} such as the phase competition in AlCoCrFeNi and FeCoNiCrMn,³⁹ Al_{0.5}CoCrFeNi,⁴⁰ and AlCoCrFeNiMo.⁴¹

Whether a phase is a solid solution or an intermetallic compound can be examined in a mixing entropy-enthalpy plane that is referred to as MEE plane. In the plane, the negative sign branch of the two critical phase boundary lines, which satisfy the critical condition of $\pm\Delta H = T\Delta S$, separates a solid solution state from an intermetallic state.⁴²

To elucidate their influence on alloys, we design an experiment to investigate how microstructure of six five-component equi-atomic HEAs of a constant configuration entropy, $R\ln 5$, changes with different mixing enthalpies, i.e., with different combinations of components from the single set of (Al, Co, Cr, Fe, Ni, Ti).

Designations such as C-6 and H-6 denote samples for as-cast and as-homo AlCoCrFeNiTi, respectively. Alloys C-5(Al) and H-5(Al) mean as-cast and as-homo CoCrFeNiTi, respectively, and so forth for other five 5-element alloys. (See Table 1.) As is seen in Figure 1, the research plan in this study has a hexagonal center of C-6. At each side of the hexagon are located respectively C-5(Ti), C-5(Al), C-5(Co), C-5(Cr), C-5(Fe), and C-5(Ni). Relevant references collected in this study are updated and listed for each of them in Figure 1. Most studies gathered on the corner of C-6, C-5(Ti), and C-5(Al). There are even no studies on C-5(Co), C-5(Cr), and C-5(Ni) for the moment. The left bottom corner of Figure 1 lists the origin and important developments, as well as Heusler research. The right bottom corner lists reviews and analyses of phase stability.

Table 2 lists related binding enthalpies between constituent elements in the alloys, the work functions and electro-negativities for constituent elements. Table 3 lists melting points, atomic radii, and the valence electron concentrations for the elements. A lattice distortion parameter δ is defined in Equation (1) as a comprehensive effect of the atomic-size difference. Another parameter, Ω , that is a measure of degree of importance between entropy and enthalpy in an alloy system, is defined as a ratio of $T\Delta S_{\text{mix}}$ to the absolute value of ΔH_{mix} .³⁴ Usually a plot of Ω

against δ is used to predict whether an HEA is a random solid solution or an intermetallic.

$$\delta = \sqrt{\sum_{i=1}^n c_i \left(1 - \frac{r_i}{\bar{r}}\right)^2}, \quad (1)$$

where $\bar{r} = \sum_{i=1}^n c_i r_i$ is an average value of atomic size; c_i and r_i are the i th element concentration and the i th element radius, respectively; and n is the number of elements in an HEA. The value of r_i can be referred to in reference.²³

2. Materials and Methods

2.1. Alloy preparation

Each sample about 40 g was put in a water-cooled Cu crucible under 0.2 atm Ar atmosphere and arc melted in an arc remelter at 420 A DC current. Ar-purge three times before melting to reduce oxidation during melting was used, and each sample was melted three times and between adjacent melting processes, the sample was turned over once to ensure complete mixture of components. After solidification, an as-cast sample was obtained. The as-cast samples for all alloys, but not for the Al-free were homogenized at 1100°C for 24 h and water quenched. The homogenization temperature for Al-free samples was 900°C. (As-cast samples were prepared in a vacuum arc remelter under Ar gas protection from 99.9 %-pure elemental

Al, Co, Cr, Fe, Ni, and Ti. As-homogenized samples were manufactured in quartz tubes at 1100°C (except for C-5(Al) which was at 900°C) for 24 h and water-cooled.

2.2. Microstructural observations

Samples for microstructural observations were cut and ground in sequence of numbers of 80, 120, 240, 400, 800, 1000, 1200, 2400, and 4000 of silicon carbide (SiC) papers; and then polished with Al₂O₃ powders from 1, 0.3, and to 0.05 μm in size. The sample surface was then ready for observations in a JEOL JSM-840A SEM.

2.3. X-ray diffraction (XRD)

A Rigaku ME510-FM2 X-ray diffractometer with copper target of K_{α1} line of wavelength of 1.54056 Å was used for X-ray diffraction. Operation condition was at 30 kV and 20 mA for 2-theta angle from 20 to 100 degrees, and the scanning speed was 4°/min. Lattice parameters are obtained from XRD patterns according to methods described in standard text books.

2.4. Hardness measurements

A Matsuzawa Seiki MV-1 hardness tester was used. Sample surface for hardness test was ground by using, in sequence, # 240, # 400, # 800, # 1000, # 1200, and # 2400 SiC papers. Loading conditions were a load of 5 kg, time for 15 s,

and loading speed at 50 μm/s. Each sample was tested at five different points and the middle three data were taken and averaged.

3. Results

3.1. Gibbs free energy

In alloy formation, the changes in entropy and enthalpy in mixing constituent elements together are expressed in terms of composition and interaction between elements as ΔS_{mix} and ΔH_{mix}, respectively, in Equations (2) and (3), where R, c_i, and ω_{ij} are respectively the gas constant, the concentration of the *i*th element, and an interaction parameter between the *i*th and the *j*th different elements in the alloy. The ω_{ij} (= 4ΔH_{AB}^{mix}) is defined as four times the change in enthalpy between the *i*th and the *j*th different elements during mixing at their liquid state, Δ(H^{ij})_{mix}.

$$\Delta S_{mix} = -R \sum_{i=1}^n c_i \ln c_i \quad (2)$$

$$\Delta H_{mix} = \sum_{i=1, i \neq j}^n \omega_{ij} c_i c_j \quad (3)$$

The change in the Gibbs free energy, ΔG_{mix}, which is defined in Equation (4),

$$\Delta G_{mix} = \Delta H_{mix} - T \Delta S_{mix}, \quad (4)$$

where T = Σ_ic_i(T_m)_i is the calculated melting temperature of an alloy. Zhang et al. have proposed the criterion relationship of ΔH_{mix-to-δ} in HEA and typical

multicomponent bulk metallic glasses⁴⁰ and δ is also discussed as a factor in the formation of solid solution for HEAs.³⁷ Yang et al. have proposed another important factor Ω , where $\Omega = \frac{T_m \Delta S_{mix}}{|\Delta H_{mix}|}$, for which alloy is a stabilized solid-solution or not.³⁴ $\Delta G_{mix} = 0$ means a reversible state; < 0 a spontaneous process (mixing of elements); and > 0 an unstable process (not mixing) for the alloy system. Utilizing the atomic size and mixing enthalpy related to this phase selection rule is discussed.

However, in HEA systems, large configuration entropy also affects the solubility of individuals in HEA, in such a way as in $\Delta G = \Delta H_{mix} - T\Delta S_{mix}$ when $\Delta G = 0$ for a reversible process in HEA mixing is the critical condition for mixing.

The changes in entropy and enthalpy in mixing alloy constituent elements together are expressed in terms of composition and interaction between elements as ΔS_{mix} and ΔH_{mix} , respectively (Table 4). The change in the Gibbs free energy, ΔG_{mix} , means the difference of $\Delta H_{mix} - T\Delta S_{mix}$ changes. The thermodynamic explanation for the simple phase diagrams is discussed for HEA systems. Senkov et al. have proposed a contradiction that solid solution alloys become less likely as the number of alloy elements increases. As the number of elements increases, the configurational entropy rises slowly.³⁶

As $\Delta G_{mix} \leq 0$, two states, a solid solution and an intermetallic, might occur. How can we differentiate the two? An alloy, being a solid solution or an intermetallic, is further determined by ΔH_{mix} . When this mixing enthalpy is very negative, the alloy must be an intermetallic, as it is slightly negative or positive, as in Ti-V, Ti-Zr, and Ti-Hf,⁴⁶ comes a solid solution. Since the ‘physical’ $T\Delta S_{mix}$, which is usually a positive term, affects the ‘chemical’ ΔH_{mix} in the mixing Gibbs free energy ΔG_{mix} . $\Delta G_{mix} = 0$ means $\Delta H_{mix} = T_m \Delta S_{mix}$, is a critical condition for an alloy to be stable or not. This condition is to plot a mixological $T\Delta S_{mix}$ -to- ΔH_{mix} diagram (referred to as a MEE plane, see below) and use a criterion for solid solution, $|\Delta H_{mix}| \leq T\Delta S_{mix}$, instead of $\Delta G_{mix} \leq 0$, to discuss the solubility of elements in HEAs. In the area of $|\Delta H_{mix}| \leq T\Delta S_{mix}$ in $T\Delta S_{mix}$ -to- ΔH_{mix} an extension of ΔH_{mix} is seen as $T\Delta S_{mix}$ increases. In doing this, one may avoid using the complex hyper-dimensional phase diagram in treating HEAs.

From six elements, Al, Co, Cr, Fe, Ni, and Ti, seven equiatomic alloys including six five-component and one six-component alloys are designed as shown in Figure 1 and Table 5. Both as-cast and as-homogenized samples are prepared and their microstructure is discussed in a designed MEE plane. The absolute value of the entropy energy (defined as entropy times melting temperature in K) to enthalpy

ratio, Ω , vs. the lattice distortion, δ , is also discussed in terms of the actual experimental composition, rather than the nominal composition. The total number of the phases of binary alloys is listed in Table 6. The main idea is to check, whether or not, both entropy and enthalpy are more important than the lattice distortion for phase stability and check the degrees of freedom in the alloys by the Gibbs phase rule. Table 1 lists designations for as-cast and as-homogenized alloys.

Figure 2 illustrates that in alloys with both Al and Ti, all but H-5(Cr), appears $L2_1$ Heusler. All alloys, other than C-5(Al) and H-5(Al) which being with A12, $D0_{24}$ and HCP, have BCC with their microstructure, meaning $L2_1$ Heusler being found in C-6, H-6, C-5(Ni), H-5(Ni), C-5(Co), H-5(Co), C-5(Fe), H-5(Fe) and C-5(Cr), totally 9 samples. $L2_1$ -type Heusler was discussed clearly.⁴⁷ Al-Ti having the lowest $\Delta H_{\text{mix}} = -30$ kJ/mol shows the microstructure of multi component alloys not only relates with configurational entropy,⁴³ but relates to the formation enthalpy (Table 2). With limited exceptions, few alloys shown in literatures (Figure 1) contain Ti and Al simultaneously, no wonder could one hardly find multi component Heusler in the literatures.

3.2. BEI (back-scattered electron image)

Figure 3 illustrates the BEI and

elemental images for all 14 as-cast and -homogenized samples. In Figure 3(a), the brightness of the images has closely relationship with content of elements in different atomic number. The brighter the areas, the higher the content of higher atomic number elements. C-6 shows the occupation by Cr and Fe (with averaging atomic number of 24) in the brightness part of BEI, while the rest part of BEI is full of Ti, Co, Ni, and Al (with averaging atomic number of 22.5). C-5(Cr) has the same tendency as C-6 with Fe (with atomic number of 26) that occupies the bright part, while Ti, Co, and Ni (with averaging atomic number of 25.7) occupy the dark part in the image. C-5(Ti) is merely a single pseudo-A2 BCC solid solution, therefore there is no pattern in the microstructure. C-5(Fe) is with bright Cr (atomic number of 24) rich phase and dark Ti, Co, Ni, and Al-rich phase (with averaging atomic number of 22.5). C-5(Co) is principally with a bright Ni (atomic number of 28) rich and a dark Cr (atomic number of 24) rich microstructure, while C-5(Ni) is principally with a bright Co (atomic number of 27) rich and a dark Cr (atomic number of 24) rich microstructure. Finally, C-5(Al) is principally with a bright Cr (atomic number of 24) rich and a dark Ti (atomic number of 22) rich microstructure.

In Figure 3(b), the as-homogenized microstructures keep basically the same morphology as that of the as-cast, although

after homogenization most of the alloys have the tendency of reconstruction in microstructure. Thus, from observations and analyses, one may conclude that component(s) with high melting point, such as Cr and Fe, and their soluble components solidify first as a primary dendrite; while others, such as Ti, Co, Ni, and Al share the inter-dendrite. After homogenization, H-6 becomes blurred; H-5(Co) becomes sharp; H-5(Fe) is still clear; and H-5(Ti) keeps its solution state. Melting point T , atomic radius R , valence electron concentration (VEC) for various elements, number of phases, microstructure and parameters for calculation, are listed in Tables 3 and 4. EDS compositions (at %) for different phases are listed in Table 7. Relevant calculated data for the HEAs are listed in Table 8.

3.3. SEM and XRD

Figure 4 shows crystal structures, diffraction peaks, and lattice parameters of the alloys. Some phases have so weak peak intensity that they cannot be calculated to obtain their lattice parameters, such as in C-5(Al) and H-5(Al). In this six-component equi-atomic alloy and its derived six five-component equi-atomic alloys, there are totally six observed phases including FCC, BCC, HCP, A12, D0₂₄ and L2₁ Heusler. Each alloy contains one to three phases. Among the 14 samples, eight have two phases; four have three phases; and two

have just one single phase. There are eight samples that simultaneously have BCC and L2₁ Heusler. According to the Gibbs phase rule, at constant pressure there are seven and six degrees of freedom for six- and five-component alloys, respectively, the samples have three to six degrees of freedom in each alloy of this study. The lattice parameter of BCC ranges from 2.878 Å to 2.940 Å, while that of Heusler ranges from 5.842 Å to 5.875 Å. The Lattice constants (Å) and density for C-x and H-x alloys are listed in Table 9.

According to SEM and XRD (Figure 4), C-5(Al) and H-5(Al) possess three phases of A12, D0₂₄ (Ni₃Ti-type) and HCP, and they are the only BCC-free alloys; C-5(Co) and H-5(Co) have two BCCs and one L2₁ (Heusler); H-5(Cr) is duplex BCC-FCC; C-5(Ti) presents only one BCC; and H-5(Ti) has both one BCC and one FCC; while C-6, H-6, C-5(Cr), C-5(Fe), H-5(Fe), C-5(Ni) and H-5(Ni) possess both a BCC and an L2₁. Totally six phases are accounted in 14 HEAs, each has only one to three phases.

3.4. The analysis from MEE plane

Figure 5 delivers an important message in MEE plane, the regions of intermetallic and solid solution are divided by $\Omega = 1$. The conditions of $\Omega > 1$ and $\Delta H_{\text{mix}} \geq 0$ define conditions for the formation of solid solution for an alloy system. If one considers that $\Omega > 1$ and

$\Delta H_{\text{mix}} < 0$ also define conditions for the formation of solid solution for an alloy system in the $T_m\Delta S_{\text{mix}}$ -to- ΔH_{mix} plot for the sake of symmetry, then one can use only condition of $\Omega > 1$ to define the condition for formation of solid solution for an alloy system in this plot. On the other hand, the conditions of $0 \leq \Omega < 1$ and $\Delta H_{\text{mix}} < 0$ define conditions in the plot of a region for the formation of intermetallics. According to this definition in the mixological entropy energy-enthalpy plot (the MEE plot), one can see that as the $T_m\Delta S_{\text{mix}}$ term grows larger, the range of the ΔH_{mix} term for maintaining alloys to be a solid solution also grows larger, i.e., as $T_m\Delta S_{\text{mix}}$ becomes larger, the ability for an alloy system to be a solid solution becomes larger. Effect of high-entropy by the multiplicity of alloys extends the solubility of alloy components. Since the configurational entropy of an equi-atomic multicomponent alloy is $R \ln(n)$, where R is the gas constant, and n is the number of components in the alloy, the designed alloys (marked as predicted) can sit randomly on the two sides of the line of $\Omega = 1$ in the MEE plot, while the actual phases sit almost in order on the two sides of $\Omega = 1$ in the MEE plot: for BCC phase on the side of $\Omega > 1$ and for intermetallic Heusler on the side of $\Omega < 1$. The experimental composition, microstructure and various parameters calculated in Figure 5 are listed in Table 8.

Inserted in MEE plane is an Ω - δ plot,

which indicates that no matter whether the lattice distortion (δ) is large (8%) or small (3%), δ does not affect the phase location in MEE plane. This elucidates for phases being a solid solution or an intermetallic, lattice distortion is not a dominant factor. It is Ω and ΔH_{mix} (positive or negative) that dominate formation of what kind of phase. ΔH_{mix} should be included simultaneously with entropy in the formation of HEA; otherwise, entropy is overemphasized.³⁶

3.5. Hardness and alloy phase

As-cast alloy is harder than as-homogenized, ranging from 500 HV to 878 HV (Figure 6). Lattice constants and density are listed in Table 9. The hardest is 878 HV for C-5(Al), which is ascribed to the precipitation of HCP phase (Table 10). Among the HEAs, C-5(Ti) is a BCC, while in alloys with both Al and Ti, high-entropy Heusler is observed.

Both entropy and enthalpy are more important than the lattice distortion (Figure 5). With the same $R \ln 5$ for these five-component alloys, there is a tendency for alloy with both Al and Ti to form a BCC and an $L2_1$. Exceptions are C-5(Co) and H-5(Co) with one $L2_1$ and two BCCs; and H-5(Cr) with only BCC and without $L2_1$. A difference between C-5(Ti) and H-5(Ti) is the existence of an FCC in H-5(Ti) and without FCC in C-5(Ti) suggesting that FCC is stable during homogenization at 1100°C. BCC-free only occurs in C-5(Al)

and H-5(Al) indicating that Al is a BCC stabilizer. A difference between C-5(Cr) and H-5(Cr) is the existence of $L2_1$ in the former and the absence of $L2_1$ in the latter, indicating that Cr plays a negative role in forming $L2_1$, and $L2_1$ disappears during homogenization. Why splitting a BCC into two BCCs in C-5(Co) and H-5(Co), however, is unknown.

4. Conclusions

HCP in C-5(Al) and H-5(Al) suggests Ti is an HCP stabilizer. Simultaneous presence of primary BCC dendrite and $L2_1$ Heusler interdendrite, according to calculation, occurs when mixing enthalpy for the latter is lower than for the former in alloys containing both Al and Ti. C-5(Al) is the hardest because of presence of $A12$, $D0_{24}$ (Ni_3Ti -type) and HCP. One-BCC alloy, e.g. C-5(Ti), is simple and convenient for study purpose.

Contributions

S.K. Chen is the principle investigator of this project. S.K. Chen and C.H. Lin designed this study. C.H. Lin conducted the experiment. S.K. Chen and P.H. Lee wrote the manuscript.

Competing financial interests

The authors declare no competing financial interests.

Acknowledgements

S.K. Chen thanks the Ministry of Science and Technology, ROC, for financial support under grant number 103-2221-E007-033-MY3. P.H. Lee would like to thank Micky Yang for a useful discussion.

References

- 1 Yeh JW, Chen SK, Lin SJ, Gan JY, Chin TS, Tsau CH, Chang SY. Nanostructured high-entropy alloys with multiple principal elements: Novel alloy design concepts and outcomes. *Adv Eng Mater.* 2004;6:299–303.
- 2 Yeh JW, Chen SK, Gan JY, Lin SJ, Chin TS, Shun TT, Tsau CH, Chang SY. Formation of simple crystal structures in Cu-Co-Ni-Cr-Al-Fe-Ti-V alloys with multiprincipal metallic elements. *Metall Mater Trans A.* 2004;35:2533-2536.
- 3 Zhang Y, Zuo TT, Tang Z, Gao MC, Dahmen KA, Liaw PK, Lu ZP. Microstructures and properties of high-entropy alloys. *Prog in Mater Sci.* 2014;61:1–93.
- 4 Lim XZ. Metal Mixology. *Nature.* 2016;533:306-307.
- 5 Chuang MH, Tsai MH, Wang WR, Lin SJ, Yeh JW. Microstructure and wear behavior of $Al_xCo_{1.5}CrFeNi_{1.5}Ti_y$ high-entropy alloys. *Acta Mater.* 2011;59:6308–6317.
- 6 Tong CJ, Chen MR, Yeh JW, Lin SJ, Chen SK, Shun TT, Chang SY. Mechanical performance of the $Al_xCoCrCuFeNi$ high-entropy alloy system with multiprincipal elements. *Metall Mater Trans A.* 2005;36A:1263-1271.
- 7 Zhou YJ, Zhang Y, Wang YL, Chen GL. Solid solution alloys of $CoCrFeNiTi_x$ with excellent room-temperature mechanic properties. *Appl Phys Lett.* 2007;90:181904.
- 8 Wen LH, Kou HC, Li JS, Chang H, Xue XY, Zhou L. Effect of aging temperature on microstructure and properties of AlCoCrCuFeNi high-entropy alloy. *Intermetallics.* 2009;17:266-269.
- 9 Chen ST, Tang WY, Kuo YF, Chen SY, Tsau CH, Shun TT, Yeh JW. Microstructure and properties of age-hardenable $Al_xCrFe_{1.5}MnNi_{0.5}$ alloys. *Mater Sci Eng A.* 2010;527:5818-5825.
- 10 Zhu JM, Fu HM, Zhang HF, Wang AM, Li H, Hu ZQ. Synthesis and properties of multiprincipal component AlCoCrFeNiSi_x alloys. *Mater Sci Eng A.* 2010;527:7210-7214.
- 11 Hsu CY, Juan CC, Wang WR, Sheu TS, Yeh JW, Chen SK. On the superior hot hardness and softening resistance of $AlCoCr_xFeMo_{0.5}Ni$ high-entropy alloys. *Mater Sci Eng A.* 2011;528:3581-3588.
- 12 Senkov ON, Wilks GB, Scott JM, Miracle DB. Mechanical properties of $Nb_{25}Mo_{25}Ta_{25}W_{25}$ and $V_{20}Nb_{20}Mo_{20}Ta_{20}W_{20}$ refractory high entropy alloys. *Intermetallics.*

2011;19:698-706.

13 Tsai MH, Wang CW, Tsai CW, Shen WJ, Yeh JW, Gan JY, Wu WW. Thermal stability and performance of NbSiTaTiZr high-entropy alloy barrier for copper metallization. *J Electrochem Soc.* 2011;158:H1161-H1165.

14 Chou YL, Wang YC, Yeh JW, Shih HC. Pitting corrosion of the high-entropy alloy $\text{Co}_{1.5}\text{CrFeNi}_{1.5}\text{Ti}_{0.5}\text{Mo}_{0.1}$ in chloride-containing sulphate solutions. *Corros Sci.* 2010;52:3481-3491.

15 Chen SK. Electrochemical passive properties of $\text{Al}_x\text{CoCrFeNi}$ ($x = 0, 0.25, 0.50, 1.00$) high entropy alloys in sulfuric acids. *Corros Resist.* 2012, Shih H (Ed.), ISBN: 978-953-51-0467-4, InTech.

16 Tong CJ, Chen YL, Chen SK, Yeh JW, Shun TT, Tsau CH, Chang SY. Microstructure characterization of $\text{Al}_x\text{CoCrCuFeNi}$ high-entropy alloy system with multiprincipal elements. *Metall Mater Trans A.* 2005;36A:881-893.

17 Zhang KB, Fu ZY, Zhang JY, Wang WM, Lee SW, Nihara K. Characterization of nanocrystalline CoCrFeNiTiAl high-entropy solid solution processed by mechanical alloying. *J Alloy Compd.* 2010;495:33-38.

18 Xia S, Yang X, Chen M, Yang T, Zhang

Y. The Al Effects of Co-Free and V-Containing High-Entropy Alloys. *Metals.* 2017;7:18.

19 Gludovatz B, Hohenwarter A, Catoor D, Chang EH, George EP, Ritchie RO. A fracture-resistant high-entropy alloy for cryogenic applications. *Science.* 2014;345:1153-1158.

20 Chen SK, Kao YF. Near-constant resistivity in 4.2-360 K in a B2 $\text{Al}_{2.08}\text{CoCrFeNi}$. *AIP Adv.* 2012;2:012111-012115.

21 Wang WR, Wang WL, Yeh JW, Phases, microstructure and mechanical properties of $\text{Al}_x\text{CoCrFeNi}$ high-entropy alloys at elevated temperatures. *J Alloy Compd.* 2014;589:143-152.

22 Chen MR, Lin SJ, Yeh JW, Chen SK, Huang YS, Tu CP. Microstructure and properties of $\text{Al}_{0.5}\text{CoCrCuFeNiTi}_x$ ($x = 0 - 2$) high-entropy alloys. *Mater Trans, JIM.* 2006;47:1395-1401.

23 Wang FJ, Zhang Y. Effect of Co addition on crystal structure and mechanical properties of $\text{Ti}_{0.5}\text{CrFeNiAlCo}$ high entropy alloy. *Mater Sci Eng A.* 2008;A496:214-216.

24 Zhou YJ, Zhang Y, Wang FJ, Chen GL. Phase transformation induced by lattice distortion in multiprincipal component

CoCrFeNiCu_xAl_{1-x} solid-solution alloys. *Appl Phys Lett*. 2008;92:241917.

25 Zhang KB, Fu ZY, Zhang JY, Wang WM, Wang H, Wang YC, Zhang QJ, Shi J. Microstructure and mechanical properties of CoCrFeNiTiAl_x high-entropy alloys. *Mater Sci Eng A*. 2009;A508:214–219.

26 Santodonato LJ, Zhang Y, Feygenson M, Parish CM, Gao MC, Weber RJK, Neufeind JC, Tang Z, Liaw PK. Deviation from high-entropy configurations in the atomic distributions of a multi-principal-element alloy. *Nat Commun*. 2015;6:5964.

27 Shun TT, Chang LY, Shiu MH. Microstructures and mechanical properties of multiprincipal component CoCrFeNiTi_x alloys. *Mater Sci Eng A*. 2012;A556:170–174.

28 Lee CF, Shun TT. Age hardening of the Al_{0.5}CoCrNiTi_{0.5} high-entropy alloy. *Metall Mater Trans A*. 2014;A45:191-195.

29 Gludovatz B, Hohenwarter A, Thurston KVS, Bei H, Wu Z, George EP, Ritchie RO. Exceptional damage-tolerance of a medium-entropy alloy CrCoNi at cryogenic temperatures. *Nat Commun*. 2016;7:10602.

30 Shun TT, Hung CH, Lee CF. The effects of secondary elemental Mo or Ti addition in Al_{0.3}CoCrFeNi high-entropy alloy on age

hardening at 700 °C. *J Alloy Compd*. 2010;495:55-58.

31 Lin CM, Tsai HL. Evolution of microstructure, hardness, and corrosion properties of high-entropy Al_{0.5}CoCrFeNi alloy. *Intermetallics*. 2011;19:288-294.

32 Ma SG, Zhang SF, Gao MC, Liaw PK, Zhang Y. A successful synthesis of the CoCrFeNiAl_{0.3} single-crystal, high-entropy alloy by Bridgman solidification. *JOM*. 2013;65:1751-1758.

33 Ma SG, Zhang SF, Qiao JW, Wang ZH, Gao MC, Jiao ZM, Yang HJ, Zhang Y. Superior high tensile elongation of a single-crystal CoCrFeNiAl_{0.3} high-entropy alloy by Bridgman solidification. *Intermetallics*. 2015;54:104-109.

34 Yang X, Zhang Y. Prediction of high-entropy stabilized solid solution in multi-component alloys. *Mater Chem Phys*. 2012;132:233–238.

35 Tsai KY, Tsai MH, Yeh JW. Sluggish diffusion in Co–Cr–Fe–Mn–Ni high-entropy alloys. *Acta Mater*. 2013;61:4887–4897.

36 Senkov ON, Miller JD, Miracle DB, Woodward C. Accelerated exploration of multi-principal element alloys with solid solution phases. *Nat Commun*. 2015;6:6529.

37 Poletti MG, Battezzati L. Electronic and thermodynamic criteria for the occurrence of

high entropy alloys in metallic systems. *Acta Mater.* 2014;75:297–306.

38 Guo S, Liu CT. Phase stability in high entropy alloys: Formation of solid-solution phase or amorphous phase. *Prog in Nat Sci: Mater Int.* 2100;21:433–446.

39 Liu WH, He JY, Zhang Y, Liu CT, Lu ZP. The phase competition and stability of high-entropy alloys. *JOM.* 2014;66:1973-1983.

40 Zhang Y, Zhou Y.J., Lin J.P., Chen G.L., Liaw P.K. Solid-solution phase formation rules for multi-component alloys. *Adv Eng Mater.* 2008;10:534-538.

41 Hsu CY, Juan CC, Chen ST, Sheu TT, Yeh JW, Chen SK. Phase diagrams of high-entropy alloy system Al-Co-Cr-Fe-Mo-Ni. *JOM* 2013;65:1829-1839.

42 Guo S, Hu Q, Ng C, Liu CT. More than entropy in high-entropy alloys: Forming solid solutions or amorphous phase. *Intermetallics.* 2013;41:96-103.

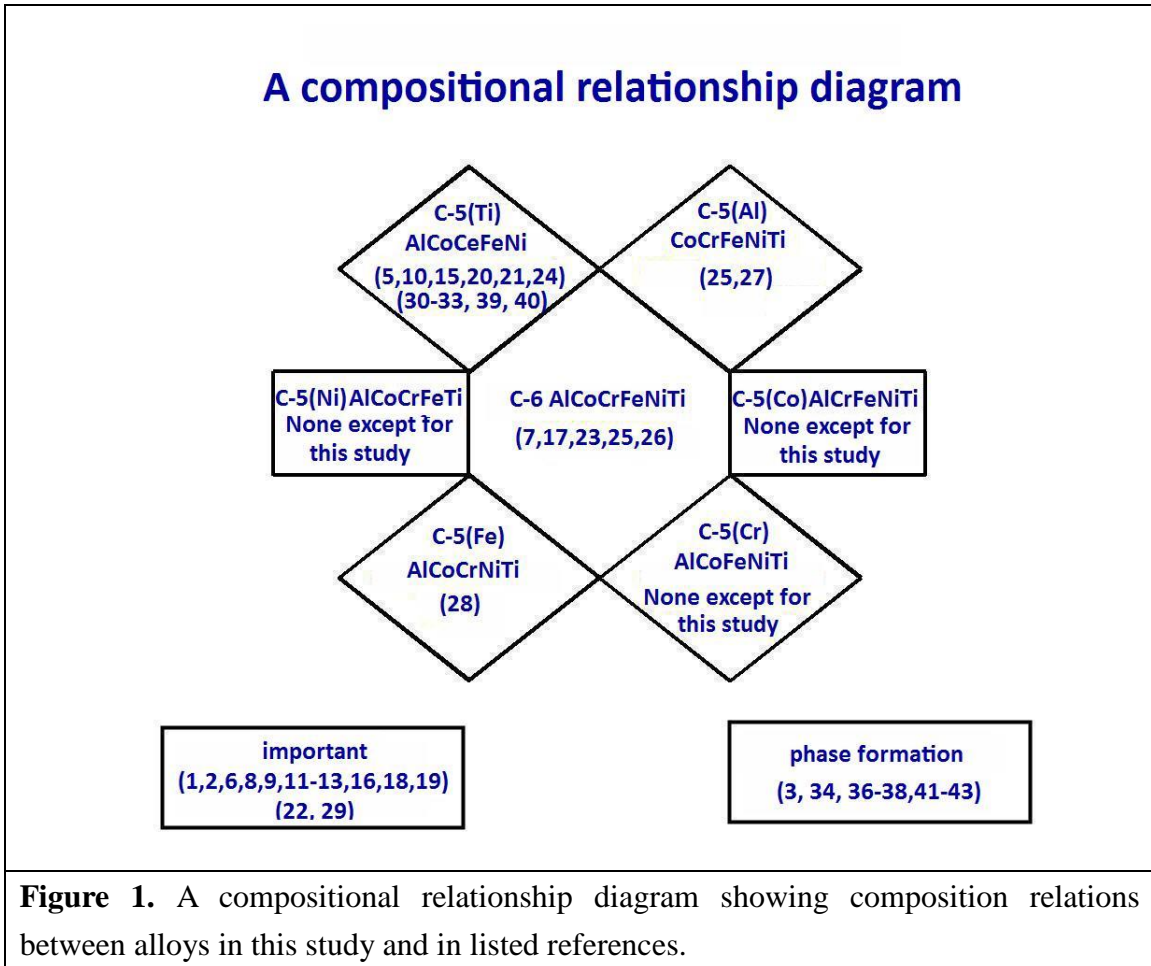
43 Takeuchi A, Inoue A. Classification of bulk metallic glasses by atomic size difference, heat of mixing and period of constituent elements and Its application to characterization of the main alloying element. *Mater Trans, JIM.* 2005;46:2817-2829.

44 Michaelson HB. The work function of the elements and its periodicity. *J Appl Phys.* 1077;48:4729-4733.

45 Kittel C., Introduction to Solid State Physics, 6th ed. (John Wiley & Sons, Inc., New York, NY, 1980).

46 Metals Handbook, 8th ed., vol. 8, Metallography, Structures and Phase Diagrams, (Metals Park, Ohio, 1973).

47 Buschow KHJ, van Engen PG. Magnetic and magneto-optical properties of heusler alloys based on aluminium and gallium. *J Mag Mag Mater.* 1981;25:90-96.



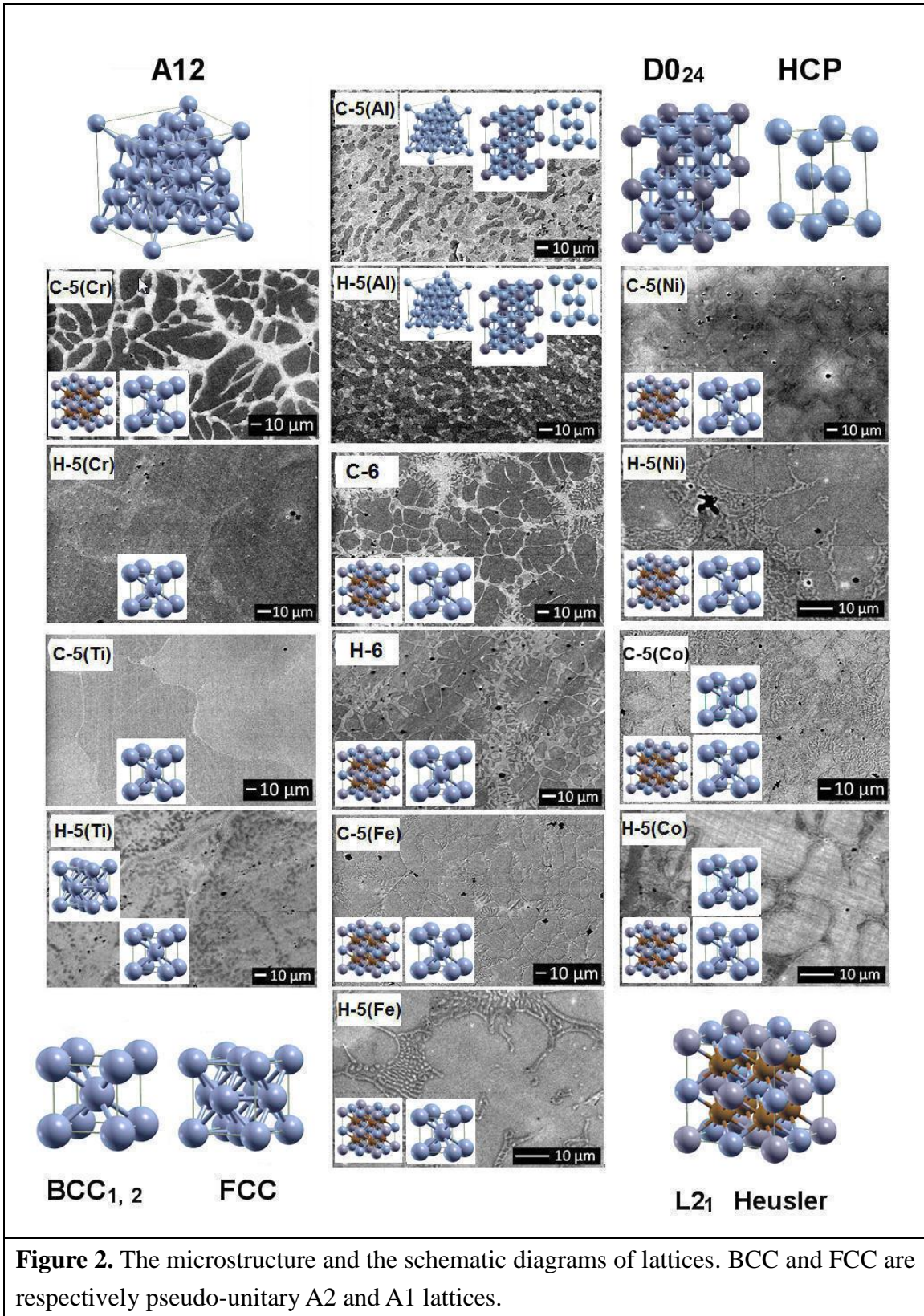


Figure 2. The microstructure and the schematic diagrams of lattices. BCC and FCC are respectively pseudo-unitary A2 and A1 lattices.

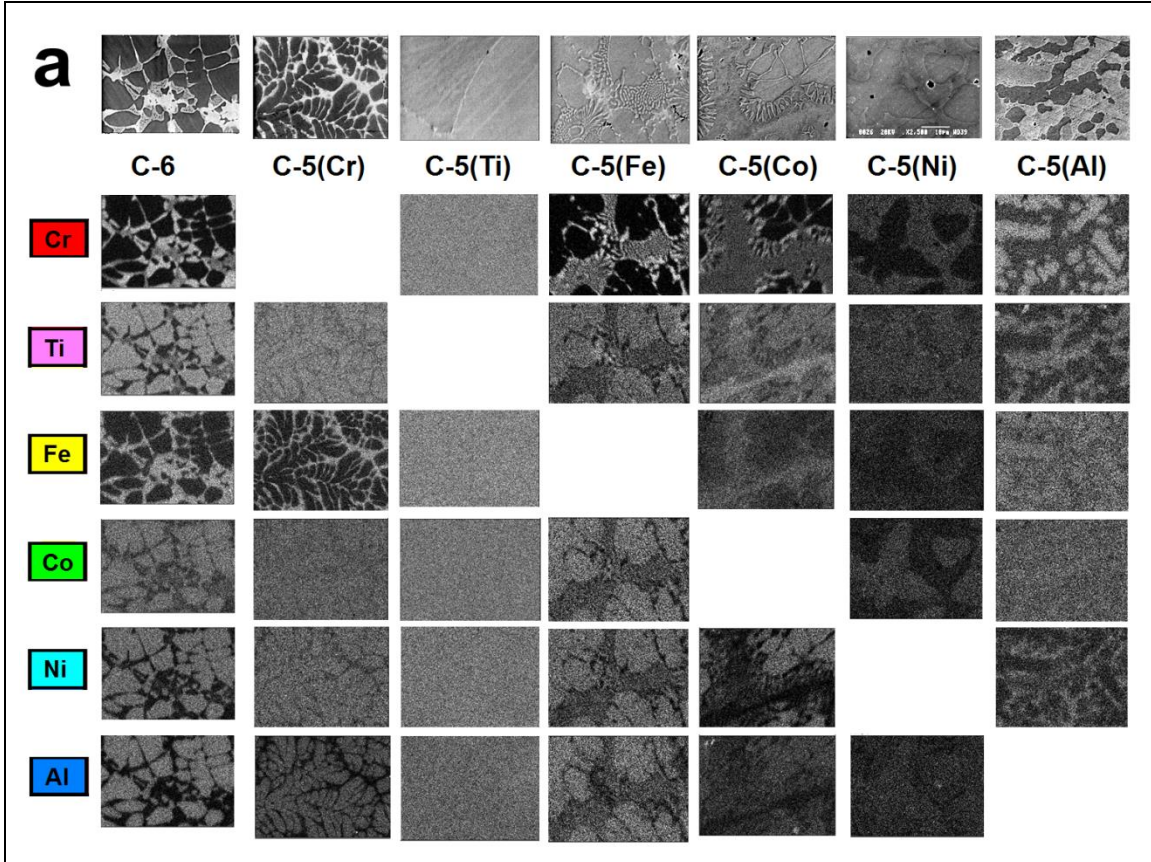
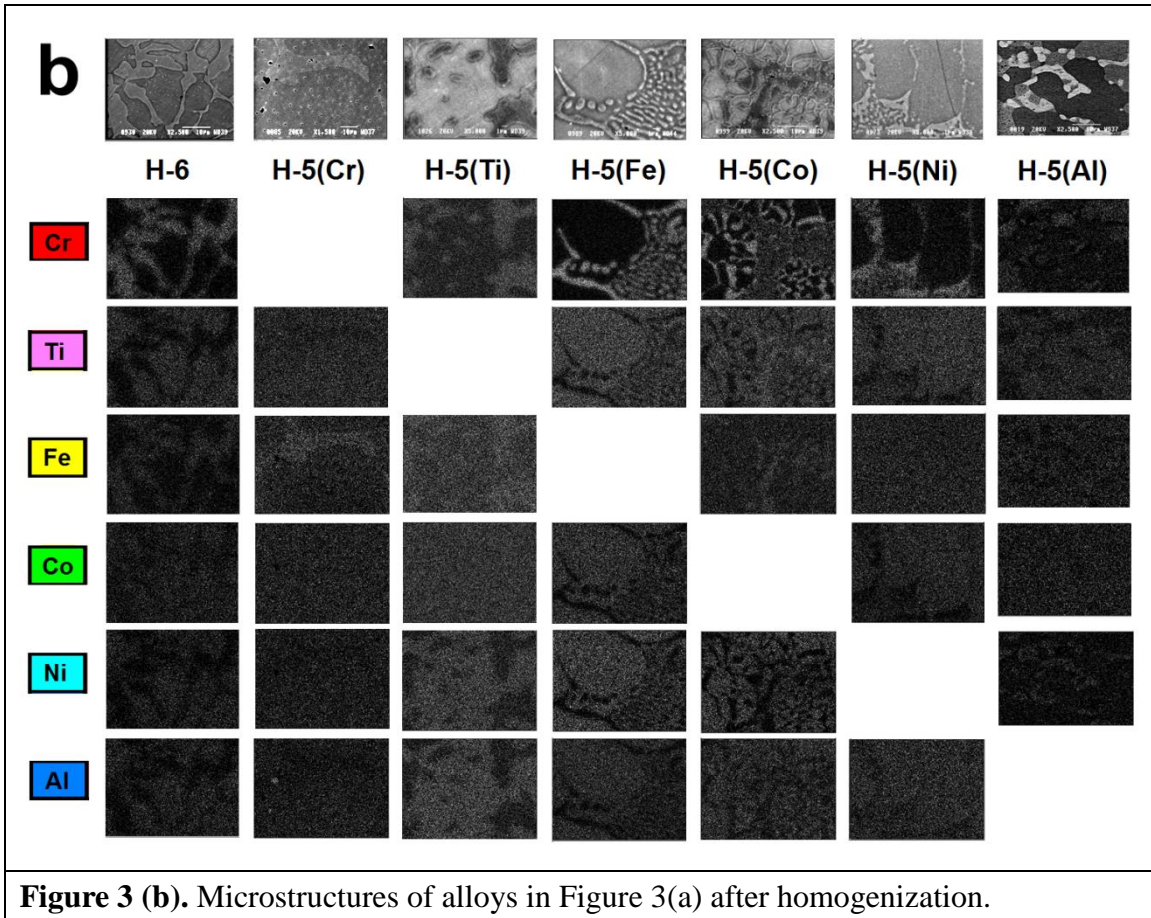


Figure 3 (a). BEI (Back-scattered electron imaging) and elemental imaging pictures of as-cast and as-homogenized six-component alloy and thereof derived six five-component equi-atomic alloys (from high to low melting point).



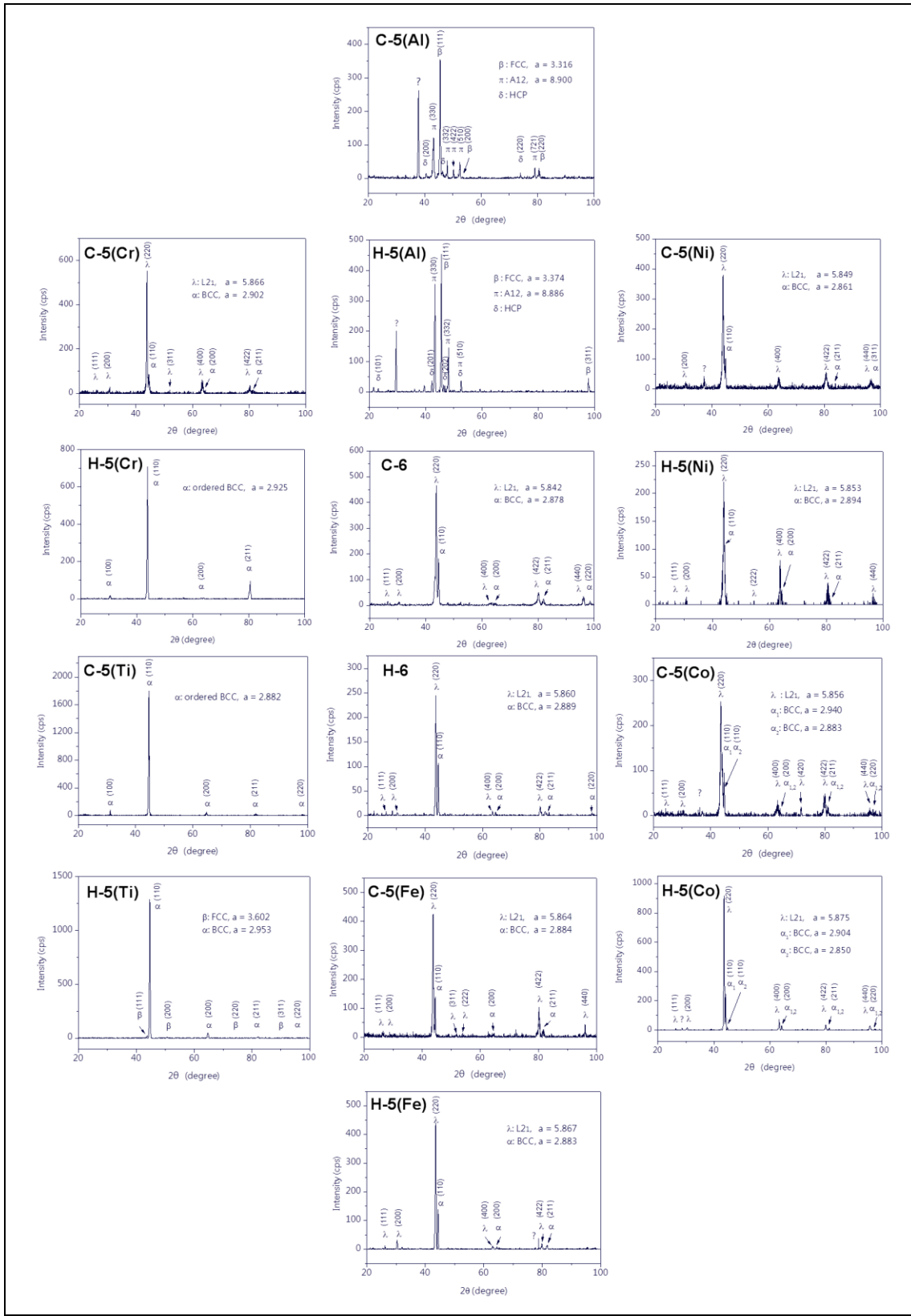
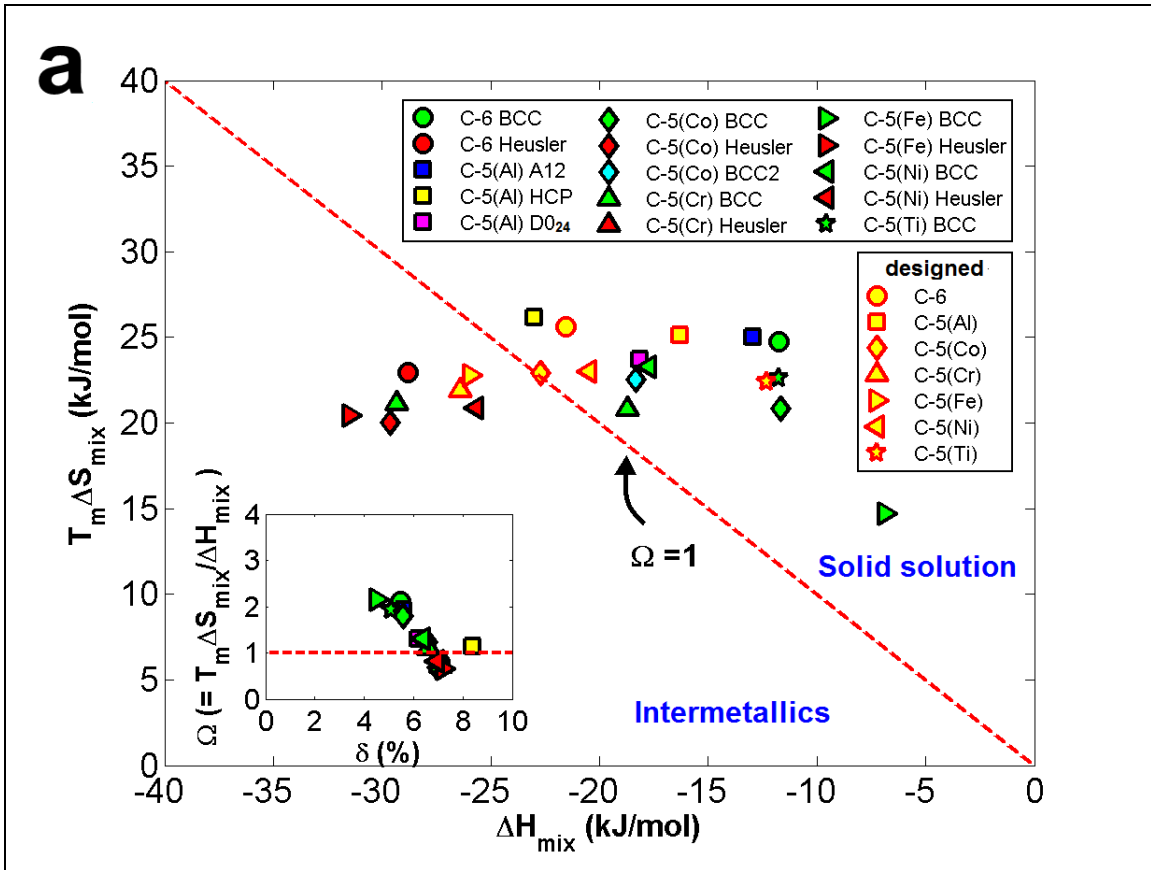


Figure 4. XRD patterns of the seven as-cast and seven as-homogenized alloys.



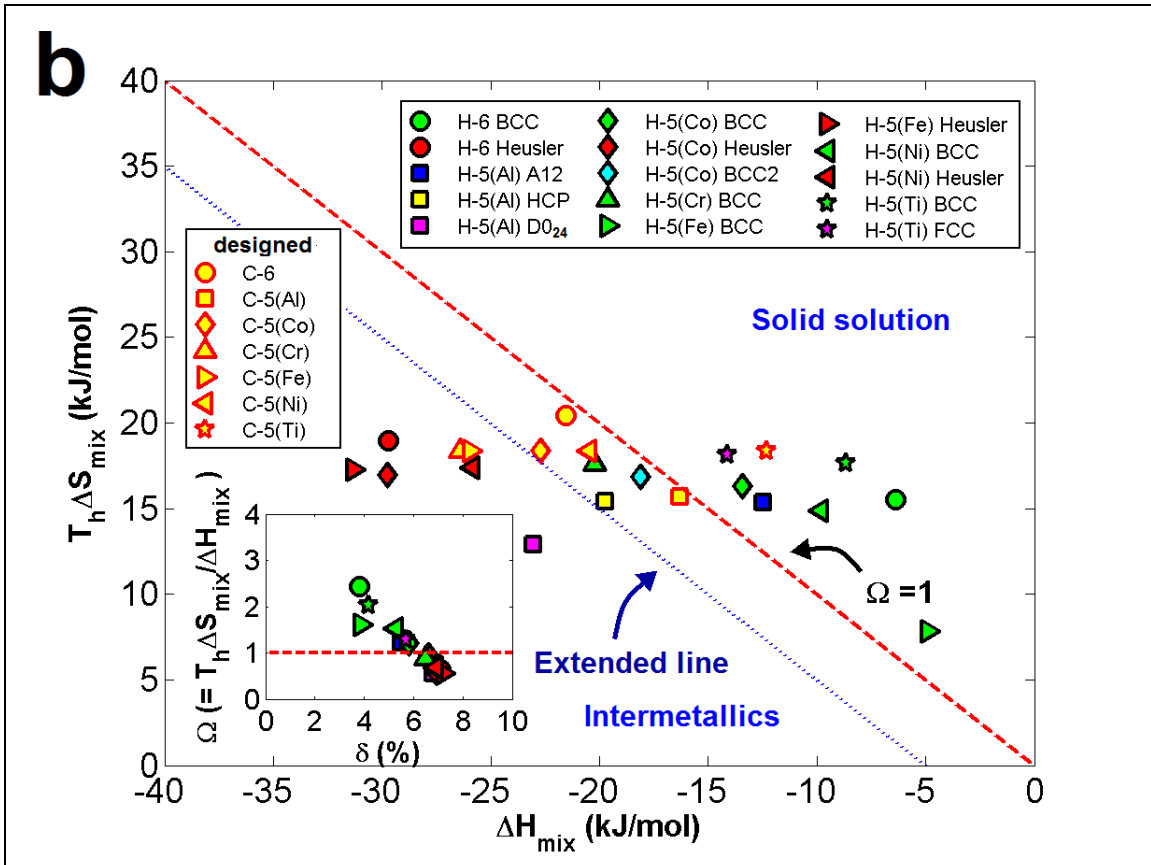


Figure 5. Distribution of as-cast (a) and as-homogenized (b) alloys in a mixological $T_m \Delta S_{mix}$ -to- ΔH_{mix} plot. While a mixed system is in equilibrium, $\Delta G_{mix} = 0$, indicating that $\Omega = T_m \Delta S_{mix} / |\Delta H_{mix}| = T_m \Delta S_{mix} / \Delta H_{mix} = 1$.

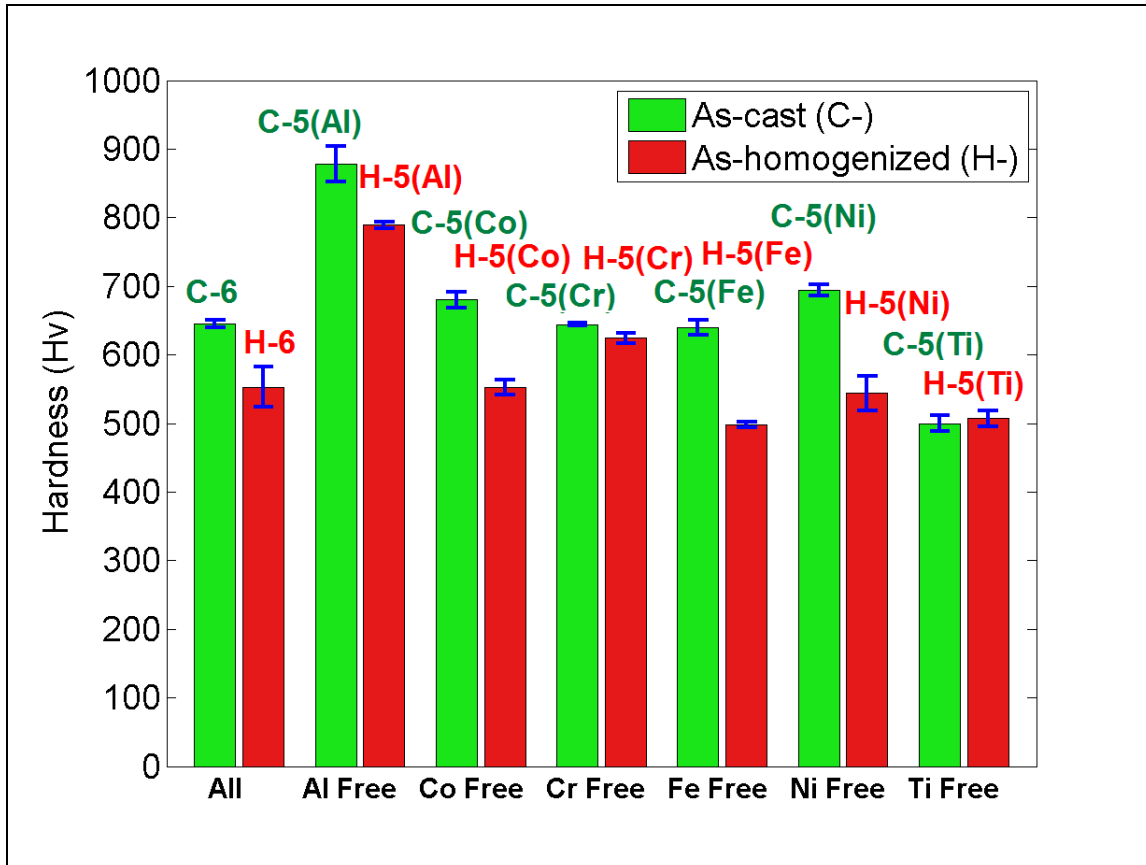


Figure 6. Hardness diagram of as-cast and as-homogenized alloys. It shows that the hardness of Al-free alloys is the highest, while that of the Ti-free is the lowest among alloys.

Table 1. Designations for as-cast and as-homogenized (as-homo) alloys in this study.

Alloy	As-cast	As-homo (1100°C)
AlCoCrFeNiTi	C-6	H-6
CoCrFeNiTi	C-5(Al)*	H-5(Al)*
AlCrFeNiTi	C-5(Co)	H-5(Co)
AlCoFeNiTi	C-5(Cr)	H-5(Cr)
AlCoCrNiTi	C-5(Fe)	H-5(Fe)
AlCoCrFeTi	C-5(Ni)	H-5(Ni)
AlCoCrFeNi	C-5(Ti)	H-5(Ti)

* “5” means 5 elements in the alloy, (Al) means Al-free in alloy and so on for the other alloys.

Table 2. The values of ΔH_{AB}^{mix} (kJ/mol) calculated by Miedema's model for atomic pairs between elements of Al, Co, Cr, Fe, Ni Ti in ref⁴³, related work function and electronegativity⁴⁴ for elements.

	Al	Co	Cr	Fe	Ni	Ti	Work function (eV)	Electronegativity
Al	-	-19	-10	-11	-22	-30	4.28	1.61
Co	-19	-	-4	-1	0	-28	5.00	1.88
Cr	-10	-4	-	-1	-7	-7	4.50	1.66
Fe	-11	-1	-1	-	-2	-17	4.50	1.83
Ni	-22	0	-7	-2	-	-35	5.15	1.91
Ti	-30	-28	-7	-17	-35	-	4.33	1.54

Table 3. The values of melting point T, atomic radius R⁴⁵ and valence electron concentration (VEC)³⁸ for elements.

	Al	Co	Cr	Fe	Ni	Ti
T (K)	933.5	1770	2133	1811	1728	1946
R (Å)	1.43	1.25	1.28	1.27	1.25	1.46
VEC	3	9	6	8	10	4

Table 4. Number of phases, microstructure and calculated ΔH_{mix} , T_m , ΔS_{mix} , ΔG_{mix} , δ (%), Ω and VEC for multicomponent HEAs.

Alloy	No. of phases	ΔH_{mix} (kJ/mol)	T_m (K)	ΔS_{mix} (J/K•mol)	ΔG_{mix} (kJ/mol)	δ (%)	Ω	VEC
C-6	2	-21.56	1720.6	14.90	-47.20	6.58	1.19	6.67
C-5(Al)	3	-16.32	1877.6	13.38	-41.44	6.13	1.54	7.40
C-5(Co)	3	-22.72	1710.3	13.38	-45.61	6.61	1.01	6.20
C-5(Cr)	2	-26.40	1637.7	13.38	-48.31	6.98	0.83	6.80
C-5(Fe)	2	-25.92	1702.1	13.38	-48.70	6.88	0.88	6.40
C-5(Ni)	2	-20.48	1718.7	13.38	-43.48	6.61	1.12	6.00
C-5(Ti)	1	-12.32	1675.1	13.38	-34.73	5.25	1.82	7.20

Table 5. Checklist for totally 57 alloy compositions out of components 1 (Al), 2 (Co), 3 (Cr), 4 (Fe), 5 (Ni), and 6 (Ti) in this study

<p>$C(6,6) = 1$ AlCoCrFeNiTi (A123456)</p>
<p>$C(6,5) = 6$ CoCrFeNiTi (A23456), AlCrFeNiTi (A13456), AlCoFeNiTi (A12456), AlCoCrNiTi (A12356), AlCoCrFeTi (A12346), and AlCoCrFeNi (A12345).</p>
<p>$C(6,4) = 15$ AlCoCrFe (A1234), AlCoCrNi (A1235), AlCoCrTi (A1236), AlCoFeNi (A1245), AlCoFeTi (A1246), AlCoNiTi (A1256), AlCrFeNi (A1345), AlCrFeTi (A1346), AlCrNiTi (A1356), AlFeNiTi (A1456), CoCrFeNi (A2345), CoCrFeTi (A2346), CoCrNiTi (A2356), CoFeNiTi (A2456), and CrFeNiTi (A3456).</p>
<p>$C(6,3) = 20$ AlCoCr (A123), AlCoFe (A124), AlCoNi (A125), AlCoTi (A126), AlCrFe (A134), AlCrNi (A135), AlCrTi (A136), AlFeNi (A145), AlFeTi (A146), AlNiTi (A156), CoCrFe (A234), CoCrNi (A235), CoCrTi (A236), CoFeNi (A245), CoFeTi (A246), CoNiTi (A256), CrFeNi (A345), CrFeTi (A346), CrNiTi (A356), and FeNiTi (A456).</p>
<p>$C(6,2) = 15$ AlCo (A12), AlCr (A13), AlFe (A14), AlNi (A15), AlTi (A16), CoCr (A23), CoFe (A24), CoNi (A25), CoTi (A26), CrFe (A34), CrNi (A35), CrTi (A36), FeNi (A45), FeTi (A46), and NiTi (A56).</p>

Table 6. Phases (totally 60) of binary alloys⁴⁶. Repeating phases are omitted.

Binary alloys	Phases	Number of phases
AlCo (A12)	α -Al, β , γ , δ , ϵ , ζ	6
AlCr (A13)	β , γ , δ , ϵ , ζ , η	6
AlFe (A14)	β , γ , δ , ϵ , ζ , η , θ	7
AlNi (A15)	β , γ , δ , ϵ	4
AlTi (A16)	β , γ , δ , ϵ , ζ , η , θ	7
CoCr (A23)	α -Co, ϵ -Co, σ , δ	4
CoFe (A24)	β , γ , δ , ϵ	4
CoNi (A25)	ϵ	1
CoTi (A26)	α -Ti, β -Ti, γ , δ , ϵ , ζ , η	7
CrFe (A34)	γ -Fe, σ	2
CrNi (A35)	α -Cr, α -Ni	2
CrTi (A36)	β , γ , δ	3
FeNi (A45)	γ' , δ	2
FeTi (A46)	ϵ , ζ	2
NiTi (A56)	β , γ , δ	3

Table 7. EDS compositions (at %) for different phases in as-cast and as-homo alloys.

Alloy	Phase	Al	Co	Cr	Fe	Ni	Ti
C-6	Cr-Fe-rich BCC	2.20	13.17	29.98	31.31	8.77	14.57
	Heusler	22.22	20.12	5.06	8.81	21.94	21.85
H-6	Cr-Fe-rich BCC	4.26	9.23	45.38	31.95	4.95	4.24
	Heusler	22.79	19.56	3.39	9.25	21.87	23.13
C-5(Al)	Cr-Fe-rich A12	0	18.94	27.98	22.77	14.43	15.89
	Ti-rich HCP	0	21.09	14.78	19.12	17.37	32.65
	Ord hex DO ₂₄ Ni ₃ Ti	0	17.81	13.20	15.17	34.47	19.36
H-5(Al)	Cr-Fe-rich A12	0	18.99	28.03	23.96	13.83	15.18
	Ti-rich HCP	0	22.49	13.86	19.61	16.39	27.64
	Ord hex DO ₂₄ Ni ₃ Ti	0	17.47	4.42	6.84	47.23	24.04
C-5(Co)	Cr-rich BCC	14.22	0	48.87	20.67	5.43	10.81
	Heusler	24.54	0	5.81	14.27	33.03	22.35
	Fe-Ti-rich BCC2	11.60	0	23.40	30.25	6.66	28.09
H-5(Co)	Cr-rich BCC	13.38	0	45.89	18.12	9.84	12.77
	Heusler	24.31	0	4.18	17.44	30.03	24.03
	Fe-Ti-rich BCC2	10.92	0	22.82	31.58	6.21	28.47
C-5(Cr)	Fe-rich BCC	3.48	16.58	0	41.49	15.43	22.60
	Heusler	23.06	22.23	0	10.93	22.58	21.21
H-5(Cr)	Fe-rich BCC	12.81	18.68	0	35.07	17.04	16.39
	FCC solid solution?	19.24	19.97	0	18.71	20.59	21.48
C-5(Fe)	Cr-rich BCC	4.21	6.91	76.01	0	4.46	8.41
	Heusler	23.12	24.43	4.80	0	23.90	23.75
H-5(Fe)	Cr-rich BCC	3.80	4.18	83.16	0	3.46	5.39
	Heusler	25.06	23.57	4.78	0	24.32	22.27
C-5(Ni)	Cr-rich BCC	17.67	16.42	27.36	20.85	0	17.70
	Heusler	22.50	31.81	7.53	14.77	0	23.39
H-5(Ni)	Cr-rich BCC	13.57	5.15	51.84	20.97	0	8.46
	Heusler	24.41	26.95	6.09	18.45	0	24.10
C-5(Ti)	Order BCC	18.28	20.44	20.08	20.94	20.40	0
H-5(Ti)	BCC	11.49	21.11	30.19	23.97	13.24	0
	FCC	24.35	19.85	15.03	16.71	24.06	0

Table 8. Microstructure and ΔH_{mix} (kJ/mol), T_m (K), ΔS_{mix} (J/K.mol), ΔG_{mix} (J/K), δ (%), Ω and VEC for multicomponent HEAs.

Alloy	Phase	ΔH_{mix}	T_m	ΔS_{mix}	ΔG_{mix}	δ	Ω	VEC
C-6	BCC	-11.73	1895	1895	-36.47	5.47	2.11	7.01
	Heusler	-28.80	1635	1635	-51.73	7.07	0.80	6.55
H-6	BCC	-6.39	1918	1918	-28.08	3.85	3.39	6.90
	Heusler	-29.72	1627	1627	-52.20	7.11	0.76	6.50
C-5(Al)	A12	-12.95	1903	1903	-37.95	5.57	1.93	7.28
	HCP	-23.01	1970	1970	-49.16	8.39	1.14	7.36
	DO ₂₄	-18.17	1844	1844	-41.87	6.19	1.30	7.83
H-5(Al)	A12	-12.49	1902	1902	-37.38	5.47	1.99	7.30
	HCP	-19.74	1870	1870	-44.32	6.80	1.24	7.17
	DO ₂₄	-23.04	1811	1811	-42.97	6.79	0.86	8.07
C-5(Co)	BCC	-11.65	1857	1857	-32.49	5.58	1.79	5.99
	Heusler	-29.64	1617	1617	-49.66	6.95	0.68	6.42
	BCC2	-18.34	1817	1817	-40.82	6.59	1.23	5.96
H-5(Co)	BCC	-13.44	1850	1850	-35.40	5.77	1.63	6.10
	Heusler	-29.74	1619	1619	-49.72	6.95	0.67	6.34
	BCC2	-18.09	1822	1822	-40.41	6.60	1.23	5.98
C-5(Cr)	BCC	-18.73	1788	1784	-39.56	6.60	1.11	7.36
	Heusler	-29.31	1610	1610	-50.45	7.12	0.72	6.67
H-5(Cr)	BCC	-20.22	1700	1699	-42.00	6.53	1.08	7.23
	FCC?.	-27.14	1646	1646	-49.14	7.04	0.81	6.79
C-5(Fe)	BCC	-6.85	2023	2023	-21.54	4.52	2.15	6.09
	Heusler	-31.46	1626	1626	-51.90	7.21	0.65	6.52
H-5(Fe)	BCC	-4.88	2048	2048	-16.53	3.87	2.39	6.04
	Heusler	-31.29	1607	1607	-51.48	7.17	0.65	6.48
C-5(Ni)	BCC	-17.72	1761	1761	-41.01	6.39	1.31	6.03
	Heusler	-25.69	1656	1656	-46.58	6.95	0.81	6.11
H-5(Ni)	BCC	-9.80	1868	1868	-30.01	5.30	2.06	6.00
	Heusler	-25.85	1638	1638	-46.59	6.89	0.80	5.96
C-5(Ti)	BCC	-11.73	1690	1690	-34.33	5.09	1.93	7.29
H-5(Ti)	BCC	-8.67	1788	1788	-31.68	4.19	2.66	7.30
	FCC	-14.13	1618	1618	-35.53	5.66	1.52	7.16

Table 9. Lattice constants (Å) and density for C-x and H-x alloys from XRD.

Alloys	L2 ₁ Heusler	BCC	BCC ₂	A12	HCP	D0 ₂₄	FCC
C-6	5.842	2.878	-	-	-	-	-
H-6	5.860	2.889	-	-	-	-	-
C-5(Al)	-	-	-	8.900	-* ¹	3.316	-
H-5(Al)	-	-	-	8.886	-* ¹	3.374	-
C-5(Co)	5.856	2.940	2.883	-	-	-	-
H-5(Co)	5.875	2.904	2.850	-	-	-	-
C-5(Cr)	5.866	2.902	-	-	-	-	-
H-5(Cr)	-	2.925	-	-	-	-	-
C-5(Fe)	5.864	2.884	-	-	-	-	-
H-5(Fe)	5.867	2.883	-	-	-	-	-
C-5(Ni)	5.849	2.861	-	-	-	-	-
H-5(Ni)	5.853	2.894	-	-	-	-	-
C-5(Ti)	-	2.882	-	-	-	-	-
H-5(Ti)	-	2.888	-	-	-	-	3.602

*¹ Not available because of too weak intensity to be measured.

Table 10. Summary in structures and hardness (HV) for C-x and H-x alloys.

Alloys	L2 ₁ Heusler	BCC	BCC ₂	A12	HCP	D0 ₂₄	FCC	Hardness (HV)
C-6	○	○						645 ± 6
H-6	○	○						553 ± 29
C-5(Al)				○	○	○		878 ± 26
H-5(Al)				○	○	○		789 ± 5
C-5(Co)	○	○	○					680 ± 12
H-5(Co)	○	○	○					553 ± 11
C-5(Cr)	○	○						644 ± 2
H-5(Cr)		○						624 ± 7
C-5(Fe)	○	○						640 ± 11
H-5(Fe)	○	○						498 ± 4
C-5(Ni)	○	○						694 ± 8
H-5(Ni)	○	○						544 ± 25
C-5(Ti)		○						500 ± 12
H-5(Ti)		○					○	507 ± 12

The symbol “○” means the phase being in existence for the alloys.